Microchimica Acta (2020) 187: 248
https://doi.org/10.1007/s00604-020-4211-1

ORIGINAL PAPER

Electrochemical synthesis of multilayered PEDOT/PEDOT-SH/Au nanocomposites for electrochemical sensing of nitrite

Yi Ge[1] · Ruxangul Jamal[1] · Ruanye Zhang[1] · Wenli Zhang[1] · Zongna Yu[1] · Yinqiang Yan[1] · Yingcheng Liu[1] · Tursun Abdiryim[1]

Received: 5 September 2019 / Accepted: 2 March 2020 / Published online: 26 March 2020
© Springer-Verlag GmbH Austria, part of Springer Nature 2020

Abstract

A multilayered film of poly(3,4-ethylenedioxythiophene)/poly(thiomethyl 3,4- ethylenedioxythiophene)/gold nanoparticle (PEDOT/PEDOT-SH/Au) nanocomposites was successfully synthesized on indium tin oxide (ITO) and glassy carbon electrode (GCE) via an electrochemical technique. The structure and morphology of the composite was characterized by FT-IR, UV-vis, EDS, XPS, and SEM analyses. The prepared multilayered PEDOT/PEDOT-SH/Au nanocomposite was used for the electrochemical catalytic oxidation of nitrite by amperometry. The results showed that the microstructures of PEDOT/PEDOT-SH/Au nanocomposites are not strongly dependent on the substrate. Fibrous PEDOT as hard template absorbed EDOT-SH on it to form porous PEDOT/PEDOT-SH. Porous structure had the advantages of large specific surface area and high porosity for nitrite ion adsorption. The thiol group in PEDOT/PEDOT-SH stabilized Au nanoparticles (NPs) effectively through Au-S bond and allowed Au NPs to have high dispersion and excellent electrocatalytic activity. The PEDOT/PEDOT-SH/Au composite prepared on GCE had a good performance in its electrochemical response to nitrite ions. PEDOT/PEDOT-SH/Au/GCE displayed a low oxidation potential (0.74 V), a fast response time (< 3 s), a low detection limit (0.051 μM), two linear ranges (0.15–1 mM and 1–16 mM), good sensitivity (0.301 μA μM^{-1} cm^{-2} and 0.133 μA μM^{-1} cm^{-2}) with good reproducibility, stability, and selectivity.

Keywords Layer-by-layer film · Thiol group functionalized PEDOT · Porous nanofiber · Gold nanoparticles · Electrochemical nitrite sensor

Introduction

Nitrite is widely used in food additives and fertilizer industries. Large amounts of nitrite in the human body can cause serious harm to human health and may lead to cancer [1–3]. The World Health Organization has fixed the maximum limit at 3 mg/L for nitrite in drinking water [4]. Therefore, it is important to establish an accurate, rapid, simple, sensitive, and selective method for the determination of nitrite in both physiological system and environmental.

Several common methods for the determination of nitrite include chemiluminescence [5], capillary electrophoresis [6], chromatography [7], fluorescence [8], and titration [9]. However, the high cost of equipment and the tedious and time-consuming testing procedures of these analytical methods hinder their wider application in practical. Electrochemical technology has the advantages of quick response, low cost, good real-time performance, low limit of detection (LOD), and excellent sensitivity and selectivity, so it is a promising method for nitrite determination [10–12]. However, the electrooxidation of nitrite on conventional electrode usually occurs at large overpotential, which would decrease the electrode accuracy and sensitivity. To overcome this problem, different kinds of chemically modified electrode were established with high sensitivity and selectivity [13–17]. Gold nanoparticles (Au NPs) are widely used as electrode modification materials due to their excellent catalytic performance [18]. However, their stability, reproducibility,

Electronic supplementary material The online version of this article (https://doi.org/10.1007/s00604-020-4211-1) contains supplementary material, which is available to authorized users.

✉ Ruxangul Jamal
jruxangul@xju.edu.cn

✉ Tursun Abdiryim
tursunabdir@sina.com.cn

[1] Key Laboratory of Petroleum and Gas Fine Chemicals, Educational Ministry of China, School of Chemistry and Chemical Engineering, Xinjiang University, Urumqi 830046, People's Republic of China

and ability to assay nitrite at low concentrations are complicated due to their tendency to aggregate [19, 20]. Previous studies have shown that the composites consisting of Au NPs and conducting polymers possess not only the properties of each component, but also the new properties with a synergistic effect [10, 21–24]. Lin et al. [22] synthesized PEDOT/Au NP composite by electropolymerization of EDOT (3,4-diethoxythiophene) in a solution containing colloidal Au NPs showing good performance of detecting nitrite. Fan et al. [23] reported Au nanoclusters (Au NCs) stabilized by bovine serum albumin doped into PEDOT by electropolymerization for electrochemical sensing of nitrite.

Conductive polymers are ideal substrates for the uniform deposition of Au NPs, and the deposition of gold nanoparticles on conductive polymers can improve the electroactive surface area, promote electrodynamics, and improve the sensitivity and selectivity of electrodes. PEDOT and its derivatives are often used as substrates to stabilize Au NPs owing to the strong interaction between S atoms in thiophene rings and Au NPs [25, 26]. Researches have shown that thiol groups–functionalized PEDOT can effectively stabilize Au NPs by Au-S bonding. This allows Au NPs to have high dispersal, size-specific physical and chemical properties, and excellent electrocatalytic activity [27]. However, EDOT adducts may change the original bulk properties of a conducting polymer [15]. EDOT can be easily electropolymerized and form porous network at relatively low potentials [26, 28], while thiomethyl 3,4-ethylenedioxythiophene (EDOT-SH) can hardly electropolymerized at relatively high potential at 1.72 V [29]. Ouyang et al. found that electrochemically polymerized PEDOT-NH_2 had a higher impedance than PEDOT, and the formation of multilayered PEDOT/PEDOT-NH_2 films can overcome the deficiency of low conductivity of PEDOT-NH_2 effectively by the covalent bonds between the polymer and indium tin oxide (ITO) surface and PEDOT layer coated on PEDOT-NH_2 [30].

Herein, we reported a three-step approach to create a multilayered PEDOT/PEDOT-SH/Au nanocomposite on glassy carbon electrode (GCE) and ITO. First, PEDOT was selected for electropolymerization onto the substrate to form a porous network structure as a bottom layer. Then, using the PEDOT porous network as a hard template, the EDOT-SH monomer was electrochemically polymerized on the hard template to form a layer-by-layer structure of PEDOT/PEDOT-SH by the adsorption of EDOT-SH on the PEDOT layer by the π-π staking between PEDOT polymer chains and EDOT-SH molecules. And, the porous networks have the advantages of large specific surface area and high porosity for ion adsorption. The Au NPs were then electrochemically deposited on PEDOT/PEDOT-SH by reducing $HAuCl_4$ to obtain multilayered PEDOT/PEDOT-SH/Au nanocomposites. The thiol group in PEDOT-SH can effectively stabilize Au NPs through Au-S bond and allows Au NPs to have high dispersion and excellent electrocatalytic activity. Based on these considerations, the multilayered PEDOT/PEDOT-SH/Au nanocomposites were electrochemically deposited on GCE and ITO to find out the relations between structural properties and electrochemical performances of nanocomposites from GCE and ITO by applying the composite for the electrochemical sensing of nitrite. Furthermore, the effect of electrode materials on the electropolymerization process, morphology, and electrochemical response of multilayered nanocomposites to nitrite ions were also studied in this research.

Experimental

Chemicals

3,4-Ethylenedioxythiophene (EDOT, > 99%), chloroauric acid hydrate ($HAuCl_4$•$4H_2O$, 99%), acetonitrile, lithium perchlorate ($LiClO_4$, > 99%), and sodium nitrite ($NaNO_2$, 99%) were purchased from Shanghai Aladdin Reagent Company (http://www.aladdin-reagent.com/). All other chemicals were analytical grade, and all aqueous solutions were prepared with double distilled water. Phosphate buffer was prepared by mixing stock standard solutions of K_2HPO_4 (> 99%) and KH_2PO_4 (> 99%). All experiments were carried out at room temperature.

Structure characterization

The FT-IR spectra of the samples were recorded on an FT-IR spectrometer (BRUKER-QEUINOX-55) using KBr disk at a resolution of 4 cm^{-1}. The UV-vis spectra of the samples were recorded by a UV-visible spectrophotometer (UV4802, Unico, USA) to determine the absorbance of polymer films deposited on ITO (Ying kou you xuan Trade co., Ltd., square resistance < 10 Ω) slides in situ directly. The morphological information of the samples was obtained by a scanning electron microscope (SEM, SO8010, Japan). Energy dispersive X-ray spectroscopy (EDS) of samples was performed with a scanning electron microscope (Hitachi, S-4800, operating voltage, 5 kV, Japan). X-ray photoelectron spectroscopy (XPS) of samples was obtained by an ESCALAB 250Xi spectrometer (Al Kα~1486.6 eV).

Preparation of the PEDOT/PEDOT-SH/Au nanocomposite

The monomer of EDOT-SH was synthesized based on a literature report [31].

PEDOT/PEDOT-SH/Au nanocomposite was prepared in three steps as follows:

First, the electropolymerization of EDOT was carried out by the cyclic voltammetry (CV) method in acetonitrile containing 5 mM EDOT and 0.1 M $LiClO_4$ between 0 and 1.5 V at a scan rate of 50 mV s^{-1} for five cycles. Then, the prepared PEDOT:ClO_4 film was labeled as PEDOT; PEDOT-modified glassy carbon electrode (PEDOT/GCE) was rinsed with acetonitrile.

Second, the PEDOT/GCE was employed as the working electrode for the electropolymerization of EDOT-SH by the CV method in acetonitrile containing 5 mM EDOT-SH and 0.1 M $LiClO_4$ between 0 and 1.5 V at a scan rate of 50 mV s^{-1} for four cycles. Then, the prepared PEDOT:ClO_4/PEDOT-SH:ClO_4 was labeled as PEDOT/PEDOT-SH; PEDOT/PEDOT-SH-modified GCE (PEDOT/PEDOT-SH/GCE) was rinsed with acetonitrile.

Finally, the electrodeposition of Au NPs was performed in a 1.0 mM $HAuCl_4$ solution with 0.1 M KCl by potentiostatic technique at the potential of − 0.5 V for 100 s. After deposition, the prepared catalyst (PEDOT/PEDOT-SH/Au/GCE) was rinsed with deionized water for several times and then dried at room temperature.

The preparation method of pure PEDOT and PEDOT-SH was the same as the above, and the total number of cycles in this process was the same. The preparation process on ITO was the same as that on the GCE.

Measurement of the electrocatalytic activity

Cyclic voltammogram experiments and amperometric measurements were performed using an electrochemical workstation CHI 660C (ChenHua Instruments Co., Shanghai, China). Electrochemical impedance tests were carried out using electrochemical workstation Zahner Zennium. A three-electrode system was employed to study the electrochemical performance of the composites. A saturated calomel electrode (SCE) was used as a reference electrode, a Pt electrode was used as a counter electrode, the PEDOT/PEDOT-SH/Au/GCE (diameter = 4 mm) and the PEDOT/PEDOT-SH/Au/ITO (length = 15 mm, width = 7 mm) were used as the working electrodes. CV measurement was performed in 0.1 M phosphate buffer (pH 6.86) containing 4 mM nitrite ion between 0 and 1 V at a scan rate of 50 mV s^{-1}. Amperometric measurement techniques were used for the quantification of nitrite ion in 0.1 M phosphate buffer (pH 6.86). Electrochemical impedance spectroscopy (EIS) test was performed in 0.1 M KCl solution containing 5.0 mM $Fe(CN)_6^{3-/4-}$ at open circuit potential in the frequency range from 0.01 to 10^5 Hz with the amplitude of 5 mV.

Results and discussion

Preparation of the PEDOT/PEDOT-SH/Au nanocomposite on the GCE and ITO surfaces

Fig S1(a) shows the electrochemical deposition process of PEDOT-SH on a bare GCE from a solution of EDOT-SH in acetonitrile containing $LiClO_4$ as supporting electrolyte by scanning the potential between 0 and 1.5 V versus the SCE reference electrode. It is clear from the first voltammetric curve that a rapid increase in the anodic current started at ~ 1.30 V, which corresponded to the beginning of the EDOT-SH monomer oxidation. The current decreases with successive potential scanning, indicating that the electropolymerization of EDOT-SH to PEDOT-SH becomes increasingly difficult. The decrease in the anodic and cathodic peak current indicated an increase in the amount of polymer on the electrode surface and the poor conductivity of PEDOT-SH.

As shown in Fig. S1(b), in the first scan of the oxidation of the EDOT-SH monomer, the radical cation on the PEDOT film forms at approximately 1.0 V which is lower than that deposited on the bare GCE. The current increases with successive potential scanning, indicating the electropolymerization of EDOT-SH to PEDOT-SH. The increase in the anodic and cathodic peak current densities suggests an increase in the amount of polymer on the electrode surface, and that the electrochemical polymerization of EDOT-SH on PEDOT is easier than that on the bare GCE. In the case of ITO (Fig.S1(d, e)), the voltammetric curves show little difference in initial oxidation potential compared with the one recorded for the GCE. The initial oxidation potential of PEDOT-SH on ITO is slightly higher than that on the GCE which indicates that the electropolymerization process does not dependent on the electrode material.

Fig. S1(c, f) shows the I-T curves of the electrodeposition of Au NPs on the PEDOT-SH and PEDOT/PEDOT-SH films. In the first few seconds, the cathodic current decreases greatly, indicating the rapid formation of gold seeds on the PEDOT/PEDOT-SH film, while the cathodic current only decreases slightly on the PEDOT-SH film due to the poor conductivity of PEDOT-SH on the bare GCE and ITO. Over the next few hundred seconds, the intensity of cathodic current decreases slowly attributing to the gold seeds grow slowly into gold nanoparticles.

Characterization of the PEDOT/PEDOT-SH/Au composite

The FT-IR spectra, UV-vis absorption spectra, and EDS of composites were shown in Fig.S2 and Fig.S3. XPS spectra were shown in Fig. 1. The wide-scan XPS spectra of PEDOT/PEDOT-SH/Au show sharp peaks at 86, 163, 284, and 532 eV corresponding to the signals of Au 4f, S 2p, C

1s and O 1s, respectively. Figure 1b–d show the high-resolution XPS spectra of the PEDOT/PEDOT-SH/Au nanocomposite. For the PEDOT/PEDOT-SH/Au nanocomposite, the Au $4f_{7/2}$ and Au $4f_{5/2}$ peaks at 84.18 and 88.08 eV indicate the presence of Au_0 (Fig. 1b). As shown in Fig. 1c, the C 1s spectra of PEDOT/PEDOT-SH and the PEDOT/PEDOT-SH/Au nanocomposites display three peaks at 284.7, 286.3, and 288 eV corresponding to the C-C, C-S, and C-O bonds, respectively. The S 2p spectra of PEDOT/PEDOT-SH/Au possesses spin-split doublet peaks at 162.4 (S $2p_{3/2}$) and 163.7 eV (S $2p_{1/2}$). This is slightly lower than PEDOT/PEDOT-SH indicating the formation of Au-S bond in PEDOT/PEDOT-SH/Au (Fig. 1d).

Figure 2a displays the SEM images of polymers and composites films from GCE and ITO, respectively. As shown in Fig. 2a, the PEDOT-SH film on a GCE is composed of particles that are closely assembled to form a relatively rough surface morphology. However, after electrochemical reduction of $HAuCl_4$, Au NPs are not clearly observed in PEDOT-SH/Au (Fig. 2d) due to the poor conductivity of PEDOT-SH on the GCE hindering the electrochemical reduction of $HAuCl_4$ to Au. This result is in accordance with the EDS results, which depicts that PEDOT-SH/Au from GCE shows low atomic percentage of Au. As shown in Fig. 2b, the PEDOT film on a GCE exhibits a porous network structure composed of nanofibers. This morphology is formed by rapid monomer initiation and polymer chain growth at a relatively high polymerization potential. This morphology of the PEDOT film is consistent with that reported for an electrochemically synthesized PEDOT film in 0.1 M TBAPC [16, 32]. After electrochemical deposition of Au on PEDOT film (Fig. 2b), the small amount of Au NPs and porous network structure PEDOT can be observed (Fig. 2e). As shown in Fig. 2e, the distribution of Au NPs on the PEDOT porous network is nonuniform and highly aggregated. As depicted in Fig. 2c, after electropolymerization of EDOT-SH on porous network structure PEDOT, the nanofibers become thick with some block structures, suggesting that the PEDOT-SH layer uniformly grows on the surface of the PEDOT layer to form a porous PEDOT/PEDOT-SH, and PEDOT/PEDOT-SH (Fig. 2f) displays more uniform distribution of Au NPs on the porous network of PEDOT/PEDOT-SH than that of PEDOT-SH/Au (Fig. 2d) and PEDOT/Au (Fig. 2e). Partial enlargement of PEDOT and PEDOT/PEDOT-SH was shown in Fig.S4.

A comparison implies that the films on GCE shows little difference from ITO indicating that the microstructures of PEDOT-SH, PEDOT, PEDOT/PEDOT-SH, and composites with Au NPs do not strongly depend on the substrate (GCE and ITO). And compared with the PEDOT-SH film on the GCE, there is massive accumulation of small particles on ITO. The morphology of PEDOT on ITO is similar to that on the GCE. After electrochemical deposition of Au on PEDOT film (Fig. 2k), nonuniform and highly aggregated Au NPs occurred in porous network of PEDOT. However, the morphology of the PEDOT/PEDOT-SH multilayer film on ITO (Fig. 2i) is different from GCE (Fig. 2c), and the

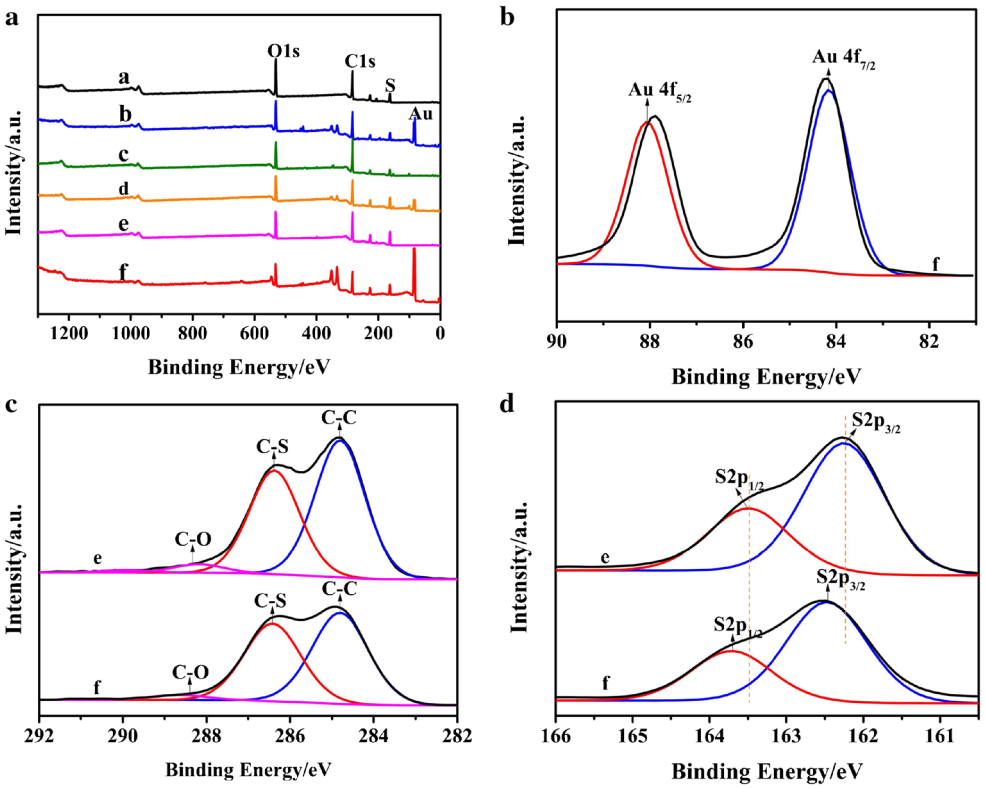

Fig. 1 XPS spectra of (**a**) PEDOT/ITO, (**b**) PEDOT/Au/ITO, (**c**) PEDOT-SH/ITO, (**d**) PEDOT-SH/Au/ITO, (**e**) PEDOT/PEDOT-SH/ITO, and (**f**) PEDOT/PEDOT-SH/Au/ ITO. High-resolution scans of (**b**) Au4f, (**c**) C1s, and (**d**) S2p

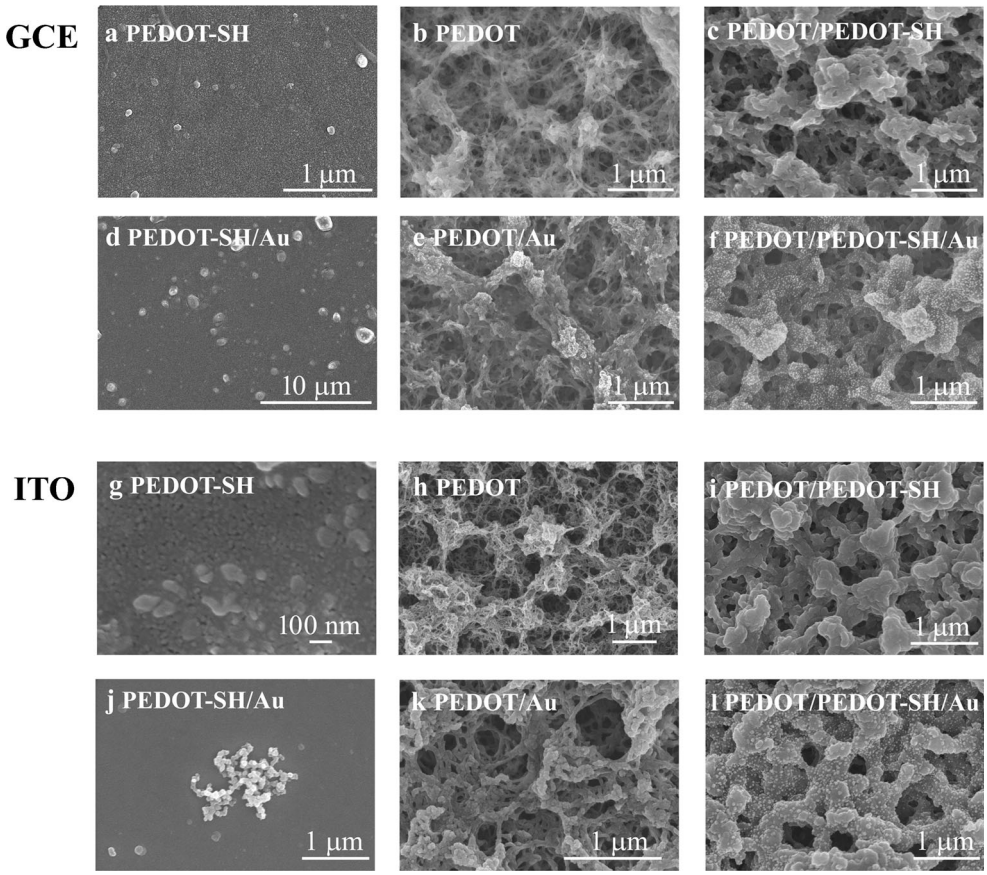

Fig. 2 SEM images of (**a**) PEDOT-SH/GCE, (**b**) PEDOT/GCE, (**c**) PEDOT/PEDOT-SH/GCE, (**d**) PEDOT-SH/Au/GCE, (**e**) PEDOT/Au/GCE, (**f**) PEDOT/PEDOT-SH/Au/GCE, (**g**) PEDOT-SH/ITO, (**h**) PEDOT/ITO, (**i**) PEDOT/PEDOT-SH/ITO, (**j**) PEDOT-SH/Au/ITO, (**k**) PEDOT/Au/ITO, (**l**) PEDOT/PEDOT-SH/Au/ITO

porous PEDOT/PEDOT-SH on ITO are thicker than those on the GCE. It is difficult to observe the fibrous structure inside the hole in the case of ITO, whereas the nanofiber can be observed clearly in the hole, in the case of the GCE. Another obvious difference is that the size of the gold obtained by electrochemical reduction on the polymer film surface on ITO is larger than that obtained on the GCE.

Scheme 1 indicates the possible formation mechanism of multilayered PEDOT/PEDOT-SH/Au. As a hard template for EDOT-SH polymerization, PEDOT first adsorbs EDOT-SH monomer on its surface by π-π stacking, and the adsorbed EDOT-SH monomers polymerized with on the surface of PEDOT, while some of them copolymerized with oligomers on the surface of PEDOT. PEDOT-SH grows uniformly on the surface of the PEDOT nanofibers and gradually results in an increase in the thickness of the fibers. When the redox reaction happens, Au nuclei will grow on the surface of the porous PEDOT/PEDOT-SH, and Au will attach to the thiol groups through Au-S bonding. Then, the Au nuclei will slowly grow into nanoparticles with low agglomeration of Au NPs because the coated PEDOT-SH layer on the PEDOT matrix reduces the conductivity of the polymer layer, while highly aggregated Au NPs occurred in porous network of PEDOT (Fig. 2e, k) resulting from its high conductivity. And the uniform

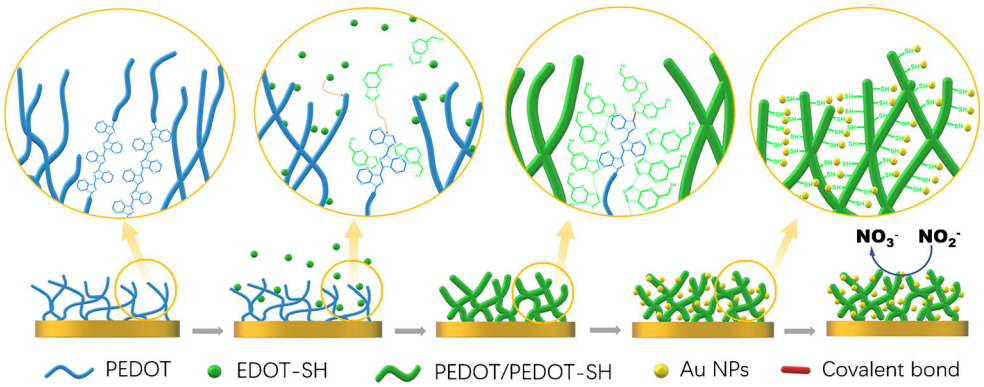

Scheme 1 The growth process of PEDOT/PEDOT-SH/Au on electrode surface

distribution of Au NPs on the porous network of PEDOT/PEDOT-SH occurred in both of GCE and ITO, suggesting that the stabilization effect of thiol group in PEDOT-SH for Au NPs through Au-S bond, allowing Au NPs to have high dispersion.

Electrochemical impedance spectra

The impedance spectra of PEDOT, PEDOT-SH, PEDOT/PEDOT-SH, PEDOT/Au, PEDOT-SH/Au, and PEDOT/PEDOT-SH/Au on the GCE (A) and ITO (B) are shown in Fig. S4. As shown in Fig. S4(a), the PEDOT coatings decrease the impedance of the GCE over the entire frequency spectrum. At lower frequencies, a great decrease in the impedance amplitude is found. However, in the case of PEDOT-SH prepared under the same conditions, the impedance of the PEDOT-SH-modified electrode is two orders of magnitude greater than that of bare GCE electrode. This result indicates that the PEDOT-SH films are not electroactive, and the PEDOT-SH coating eventually hinders charge transport. The PEDOT-SH layer deposited on the PEDOT-modified electrodes can also decrease impedance, which is similar to the phenomenon observed for PEDOT. It should be noted that the impedance of PEDOT/Au, PEDOT-SH/Au, and PEDOT/PEDOT/Au decreases significantly at lower frequencies with the presence of Au indicating that the Au NPs effectively promote charge transport. The impedance on ITO is similar to that on GCE (Fig.S4(b)).

Electrocatalytic oxidation of nitrite with PEDOT/PEDOT-SH/Au/GCE and PEDOT/PEDOT-SH/Au/ITO

Figure 3a shows the CV curves of PEDOT, PEDOT/Au, PEDOT-SH, PEDOT-SH/Au, PEDOT/PEDOT-SH, and PEDOT/PEDOT-SH/Au-modified GCEs in the presence of 4 mM nitrite in 0.1 M phosphate buffer (pH 6.86) at a scan rate of 50 mV s^{-1}. Figure 3a clearly shows that the PEDOT-SH/GCE does not show a significant anodic peak current for nitrite because of its low conductivity. However, the PEDOT-SH/Au-modified GCE exhibits a feeble broad oxidation peak current at 0.85 V due to the electrocatalytic capability of Au NPs for nitrite. In comparison with PEDOT-SH/GCE, the PEDOT and PEDOT/PEDOT-SH-modified GCEs exhibit well-defined oxidation peaks at 0.73 V and 0.74 V, with a prominent increase in the oxidation peak current. This enhancement in the peak current and oxidation peak potential can be attributed to the ideal electrocatalytic performance and high conductivity of PEDOT, which results from the deposition of PEDOT-SH on the PEDOT film enhancing its conductivity and electrocatalytic activity. After the deposition of Au nanoparticles on PEDOT and PEDOT/PEDOT-SH, the oxidation peak current significantly increases. The oxidation peak currents of the PEDOT/Au and PEDOT/PEDOT-SH/Au-modified GCEs are higher than those of the electrode without Au NPs deposition. The oxidation peak current of the PEDOT/PEDOT-SH/Au-modified GCE is higher than that of PEDOT/Au, which is attributed to the uniform distribution of Au NPs on PEDOT-SH. The electrochemical behavior of the same materials on ITO for the oxidation of nitrite is different from that on the GCE. As shown in Fig. 3b, the current response signals of these material-modified ITO electrodes with nitrite are stronger than those of the GCEs, and the oxidation potential is higher than that of the GCEs. The PEDOT-SH and PEDOT-SH/Au-modified ITO electrodes have the lowest current response among the polymers and composites on the GCEs and ITO electrodes. However, PEDOT/PEDOT-SH and PEDOT/PEDOT-SH/Au have a relatively small current response and lower oxidation potential than PEDOT and PEDOT/Au. This property should be due to the thicker PEDOT-SH layer coated on the PEDOT nanofiber, causing a decrease in the conductivity of the composite. The CV of the PEDOT/PEDOT-SH/Au in saturated nitrogen and saturated oxygen is shown in Fig. S6. The results showed that the

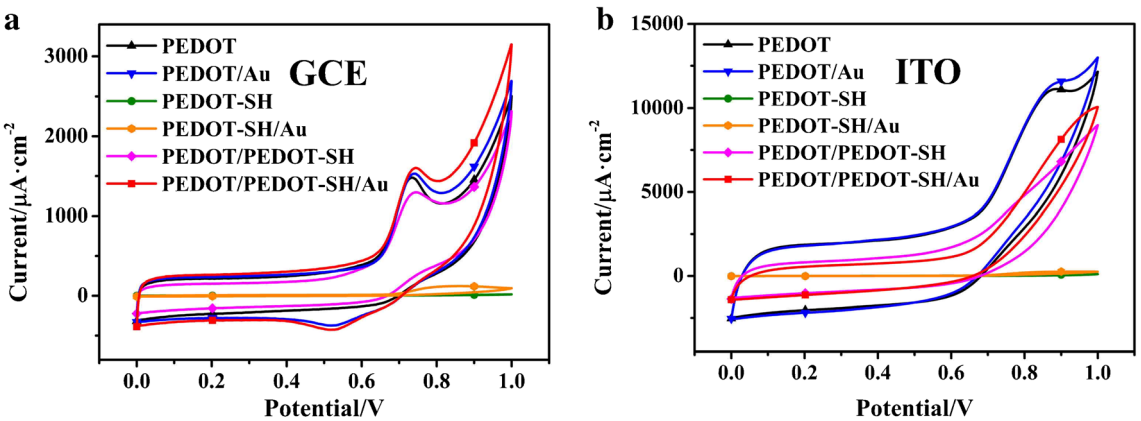

Fig. 3 Cyclic voltammograms of PEDOT, PEDOT/Au, PEDOT-SH, PEDOT-SH/Au, PEDOT/PEDOT-SH, and PEDOT/PEDOT-SH/Au in 0.1 M phosphate buffer (pH 6.86) containing 4 mM $NaNO_2$ on (**a**) GCE and (**b**) ITO at scan rate of 50 mV s^{-1}

PEDOT/PEDOT-SH/Au/GCE did not respond to the oxygen dissolved in the solution, suggesting that the dissolved oxygen has no effect on the electrochemical detection of nitrite.

Amperometric sensing of nitrite

The amperometry measurement was used on electrochemical oxidation of nitrite (Fig. 4) with the PEDOT/PEDOT-SH/Au-modified GCE and ITO for the successive addition of nitrite in 0.1 M phosphate buffer (pH 6.86) at potentials of 0.74 V and 0.95 V under stirring conditions. For the PEDOT/PEDOT-SH/Au-modified GCE, after adding nitrite, the current response of the PEDOT/PEDOT-SH/Au/GCE increases rapidly and reaches a stable state within 3 s (Fig. S7). Furthermore, this rapid increase in response to nitrite at the PEDOT/PEDOT-SH/Au-modified GCE is proportional to the concentration of nitrite. The corresponding calibration plot for the response of nitrite is presented in Fig. 4b. The amperometric response is linear with an increase in the peak current for the nitrite concentration over the ranges from 0.15 to 1 mM and 1 to 1.6 mM. The linear regression equation for the calibration plot can be expressed as $j(\mu A\ cm^{-2}) = 0.301\ C_{nitrite}(\mu M) + 7.350$ ($R^2 = 0.996$) and $j(\mu A\ cm^{-2}) = 0.133\ C_{nitrite}(\mu M) + 236.054$ ($R^2 = 0.995$) with sensitivity of 0.301 $\mu A\ \mu M^{-1}\ cm^{-2}$ and 0.133 $\mu A\ \mu M^{-1}\ cm^{-2}$, respectively. A detection limit of 0.051 μM was calculated from 3 (S/N), where S is the standard deviation of the blank signal, and N is the slope of the calibration plot. The standard error of slope and intercept of regression equations was shown in Table S1.

Compared with the PEDOT/PEDOT-SH/Au-modified GCE, the modified ITO electrode has a small current response for nitrite oxidation (Fig. 4c, d). After adding nitrite, the current response of the modified electrode increases slowly and hardly reaches a stable state. The amperometric response was found to be linear with an increase in the current for the nitrite concentration over the ranges from 40 to 1 mM and 1 to 1.6 mM, but the linear relationship is relatively poor. The linear regression equation for the calibration plot can be expressed as $j(\mu A\ cm^{-2}) = 0.005\ C_{nitrite}(\mu M) + 44.333$ ($R^2 = 0.81$) and $I(\mu A) = 0.000383 C_{nitrite}(\mu M) + 49.804$ ($R^2 = 0.92$) with sensitivity of 0.005 $\mu A\ \mu M^{-1}\ cm^{-2}$ and 0.000383 $\mu A\ \mu M^{-1}\ cm^{-2}$, respectively. Based on the above experimental results, the PEDOT/PEDOT-SH/Au/GCE with good performance was chosen for the following test.

The related data for the performance of the present sensor compared with the other previously reported sensors for the

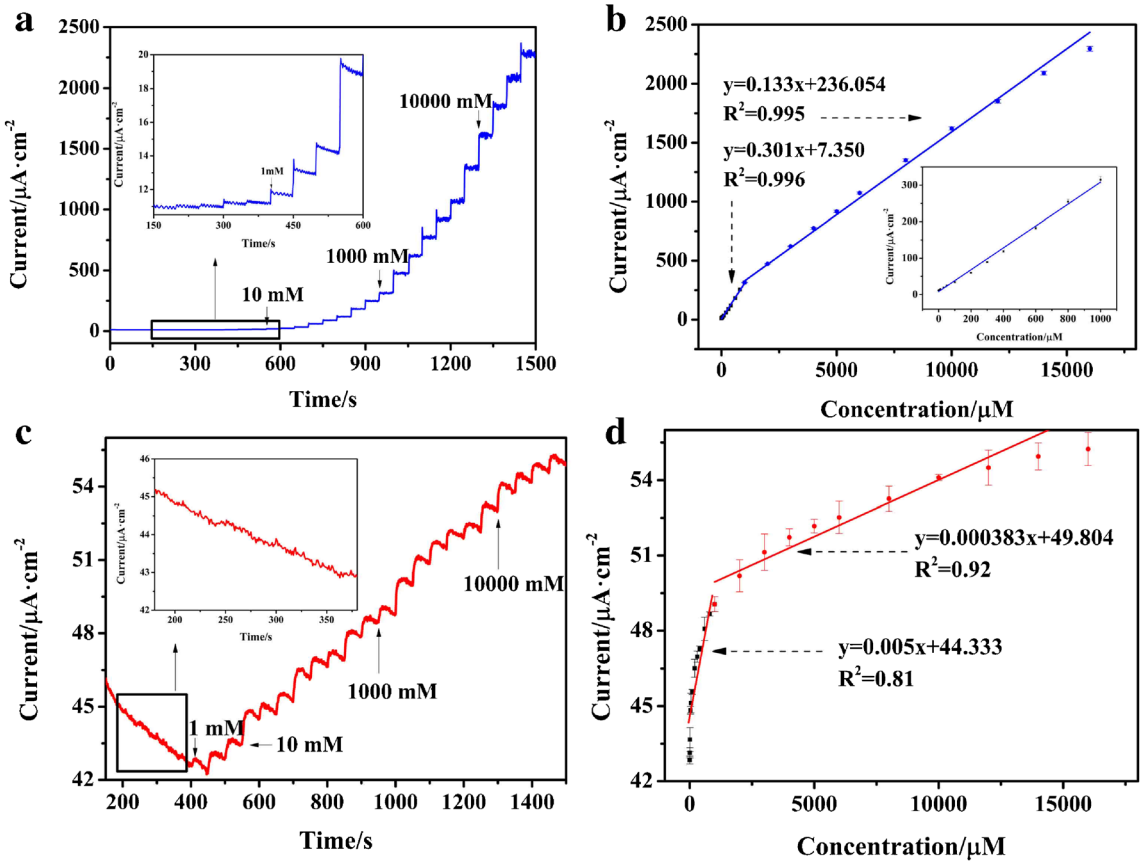

Fig. 4 Amperometric responses corresponding to consecutive additions of standard solutions of nitrite to a stirred 0.1 M phosphate buffer using the PEDOT/PEDOT-SH/Au-modified (**a**) GCE and (**c**) ITO biased at 0.74 V and 0.95 V, respectively. Calibration plot of current versus concentration of NO^{2-} (**b**, **d**)

Table 1 Comparison of the analytical performance of the various material-modified electrodes for nitrite detection

Modified electrode	Method	Potential (V)	Liner range (μM)	LOD (μM)	Sensitivity (μA $μM^{-1}$ cm^{-2})	Ref.
AuNPS-PEDOT /PMo_9V_3/GCE	CV	0.9	0.0025–1430	0.001	0.67	[10]
PEDOT/AuNP	AMP	0.8	0.2–1400	0.06	-	[22]
PEDOT/AuNCs	AMP	0.8	0.05–2600	0.017	-	[23]
PEDOT-Au	AMP	0.78	3–300	0.1	-	[24]
PANI/ABS/GCE	DPV	-	0.3–35 100–1000	0.48	23.04 0.8	[33]
Au/PANI/SnO_2/GCE	AMP	0.9	0.25–2400	0.08	0.00008314	[34]
CQD-PEDOT	AMP	0.8	0.50–1110	0.088	0.01436	[35]
GO-Ag	LSV	-	1–1000	0.24	-	[36]
Pt/CoO/GCE	AMP	0.9	0.2–3670 3670–2370	0.067	0.9014 0.4085	[37]
$NiFe_2O_4$-CPE	AMP	0.85	0.1–1000	0.1236	7.9617	[38]
rGO-MoS_2-PEDOT	DPV	-	1–1000	0.059	874.19	[39]
ZnS	AMP	0.85	0.02–1350	0.0085	-	[40]
PEDOT/PEDOT-SH/Au /GCE	AMP	0.74	0.15–1000 1000–16,000	0.051	0.301 0.133	This work

detection of nitrite are listed in Table 1. The LOD and liner range of present sensor is comparable with other sensor materials but not the best [10, 22–24, 33–40]. The performance of PEDOT/PEDOT-SH/Au/GCE in LOD is better than that of the electrode materials except AuNPS-PEDOT/PMo_9V_3/GCE [10], PEDOT/AuNCs [23], and ZnS [40]. However, it should be noted that the working potential of PEDOT/PEDOT-SH/Au/GCE is 0.74 V, which is lowest than that of electrode materials in Table 1. Furthermore, the best LOD in AuNPS-PEDOT/PMo_9V_3/GCE [10] compared with that of others may be affected when using in an alkaline condition, in which the acidic character of doping agent of heteropoly acid can decrease the electroactivity of composite material. This indicates the practical use of PEDOT/PEDOT-SH/Au/GCE in nitrite sensor. The linear range of detection is wide, and the LOD is lower than 3 mg/L of the World Health Organization fixed. This suggests that the modified GCE provided a good platform for the effective recognition of nitrite in water samples at low concentration ranges. The sensitivity of present senor are not very well compared with others reported.

Reproducibility, stability, and selectivity of PEDOT/PEDOT-SH/Au/GCE

The interference experiments of nitrite detection were carried out in order to evaluate the selectivity of the prepared sensor. As shown in Fig. 5a, PEDOT/PEDOT-SH/Au/GCE shows an obvious response toward 10 μM $NaNO_2$ and an unobvious current change toward 100 μM various common ions (i.e., Na^+, Ca^+, Mg^{2+}, Zn^{2+}, CO_3^{2-}, NO_3^-, and BrO_3^-), 100 μM various metal ions (i.e., Fe^{3+}, Cu^{2+}, and Pb^{2+}), 100 μM physiological interference (i.e., glucose and uric acid), 100 μM drug paracetamol, and 100 μM flavonoid quercetin. But for 100 μM dopamine and ascorbic acid, there are obviously

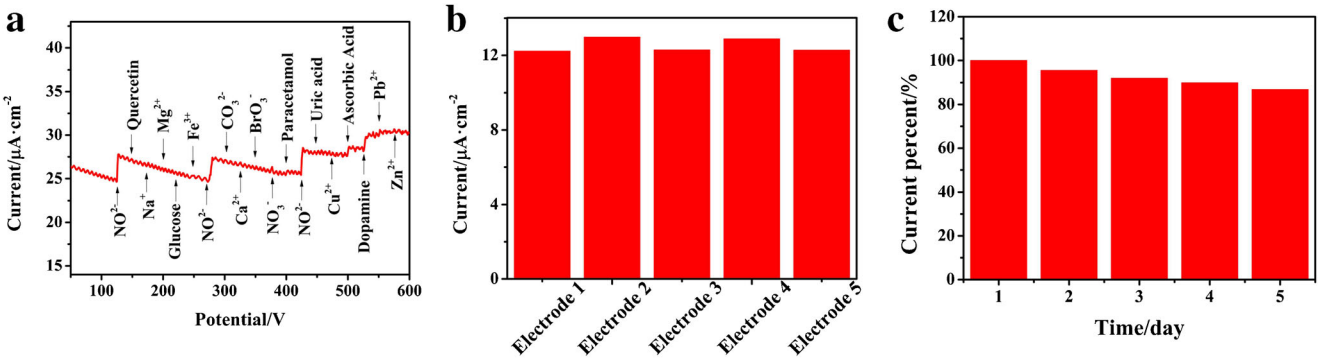

Fig. 5 **a** Amperometric measurements performed with the PEDOT/PEDOT-SH/Au-modified GCE biased at 0.74 V during consecutive addition of 100 μM different compounds tested as interferants and 10 mM nitrite to a stirred 0.1 M phosphate buffer. **b** Amperometric responses for 50 mM nitrite recorded with 5 different PEDOT/PEDOT-SH/Au/GCE prepared by using the same electrodeposition conditions. **c** Amperometric response of the PEDOT/PEDcOT-SH/Au/GCE in 0.1 M phosphate buffer with 50 mM nitrite in a period of 5 days

current response. Fortunately, the oxidation peak potentials of dopamine, ascorbic acid, and nitrite differ considerably, i.e., 0.15 V, 0.28 V, and 0.72 V (versus SCE), respectively, as shown in the differential pulse voltammetry (DPV) curve which can distinguish them very well (Fig.S8). The results demonstrate that the PEDOT/PEDOT-SH/Au/GCE sensing platform possesses good selectivity for the determination of nitrite.

The reproducibility of the PEDOT/PEDOT-SH/Au/GCE sensing platform was estimated by the analysis of the amperometric responses of 50 μM nitrite for five independently prepared PEDOT/PEDOT-SH/Au/GCE. As shown in Fig. 5b, the relative standard deviation (RSD) of these current responses is 2.9%, indicating that the PEDOT/PEDOT-SH/Au/GCE sensing platform possesses idol reproducibility for nitrite determination of nitrite.

Furthermore, the long-term stability of the PEDOT/PEDOT-SH/Au/GCE sensing platform was investigated (Fig. 5c). The stability of the sensor was tested by measuring the current response toward 50 μM nitrite after long-term storage at room temperature. Nitrite ions were measured once a day, and the current remained at about 88% of the original value after 5 days. It is the evidence of the good long-term stability of the PEDOT/PEDOT-SH/Au/GCE sensor.

Real sample analysis

In order to evaluate the usefulness of the PEDOT/PEDOT-SH/Au/GCE in practical applications, the performance of the sensor was tested with tap waters and milk samples. The standard addition method was used to determine the nitrite in tap water and milk samples; the Griess assay method was employed for the determination of nitrite ion present in the same samples and compared with the amperometric results (Table S2).

Conclusions

In summary, a reliable electrochemical nitrite sensor of PEDOT/PEDOT-SH/Au/GCE was successfully prepared via an electrochemical technique. Systematical investigations revealed that microstructures of PEDOT/PEDOT-SH/Au nanocomposites are not strongly dependent on the substrate. Fibrous PEDOT as hard template can absorb EDOT-SH on it to form porous PEDOT/PEDOT-SH which had the advantages of large specific surface area and high porosity for nitrite ion adsorption. The thiol group in PEDOT/PEDOT-SH can effectively stabilize Au NPs through Au-S bond and allows Au NPs to have high dispersion and excellent electrocatalytic activity. The PEDOT/PEDOT-SH/Au/GCE has a good performance in its electrochemical response to nitrite ions with low oxidation potential, low detection limit, and two wide linear ranges. It also exhibited good reproducibility, stability, selectivity, and detective performance of nitrite in tap water and milk samples. Nevertheless, the sensitivity of the current system needs to be further improved for trace detection.

Funding information We gratefully acknowledge the financial support from the National Natural Science Foundation of China (No. 21764014, No. 21564014).

Compliance with ethical standards

Conflict of interest The author(s) declare that they have no competing interests.

References

1. Manassaram DM, Backer LC, Moll DM (2006) A review of nitrates in drinking water: maternal exposure and adverse reproductive and developmental outcomes. Environ Health Perspect 114:320–327
2. Chen Z, Zhang Z, Qu C, Pan D, Chen L (2012) Highly sensitive label-free colorimetric sensing of nitrite based on etching of gold nanorods. Analyst 137:5197–5200
3. Parsaei M, Asadi Z, Khodadoust S (2015) A sensitive electrochemical sensor for rapid and selective determination of nitrite ion in water samples using modified carbon paste electrode with a newly synthesized cobalt(II)-Schiff base complex and magnetite nanospheres. Sensors Actuators B Chem 220:1131–1138
4. Adarsh N, Shanmugasundaram M, Ramaiah D (2013) Efficient reaction based colorimetric probe for sensitive detection, quantification, and on-site analysis of nitrite ions in natural water resources. Anal Chem 85:10008–10012
5. Lin Z, Xue W, Chen H, Lin JM (2011) Peroxynitrous-acid-induced chemiluminescence of fluorescent carbon dots for nitrite sensing. Anal Chem 83:8245–8251
6. Morcos E, Wiklund NP (2015) Nitrite and nitrate measurements in human urine by capillary electrophoresis. Electrophoresis 22:2763–2768
7. Kaku S, Tanaka M, Muramatsu M, Otomo S (2010) Determination of nitrite by high-performance liquid chromatography system with electrochemical detector: measurement of nitric oxide synthase activity in rat cerebellum cytosol. Biomed Chromatogr 8:14–18
8. Zhang H, Kang S, Wang G, Zhang Y, Zhao H (2016) Fluorescence determination of nitrite in water using prawn-shell derived nitrogen-doped carbon nanodots as fluorophores. ACS Sensors 7:875–881
9. He ZK, Fuhrmann B, Spohn U (2000) Precise and sensitive determination of nitrite by coulometric backtitration under flow conditions. Fresenius J Anal Chem 367:264
10. Zuo J, Zhang Z, Jiao J, Pang H, Zhang D, Ma H (2016) Sensitive and selective nitrite sensor based on phosphovanadomolybdates $H_6[PMo_9V_3O_{40}]$, poly(3,4-ethylenedioxythiophene) and Au nanoparticles. Sensors Actuators B Chem 236:418–424
11. Li SS, Hu Y-Y, Wang A-J, Weng X, Chen J-R, Feng J-J (2015) Simple synthesis of worm-like Au–Pd nanostructures supported on reduced graphene oxide for highly sensitive detection of nitrite. Sensors Actuators B Chem 208:468–474
12. Sheng Q, Liu D, Zheng J (2017) A nonenzymatic electrochemical nitrite sensor based on Pt nanoparticles loaded $Ni(OH)_2$/multi-walled carbon nanotubes nanocomposites. J Electroanal Chem 796:9–16
13. Ying W, Li Y, Tang L, Lu J, Li J (2009) Application of graphene-modified electrode for selective detection of dopamine. Electrochem Commun 11:889–892

14. Ko E, Tran V-K, Son SE, Hur W, Choi H, Seong GH (2019) Characterization of Au@PtNP/GO nanozyme and its application to electrochemical microfluidic devices for quantification of hydrogen peroxide. Sensors Actuators B Chem 294:166–176
15. Goda T, Toya M, Matsumoto A, Miyahara Y (2015) Poly(3,4-ethylenedioxythiophene) bearing phosphorylcholine groups for metal-free, antibody-free, and low-impedance biosensors specific for C-reactive protein. ACS Appl Mater Interfaces 7:27440–27448
16. Belaidi FS, Civélas A, Castagnola V, Tsopela A, Mazenq L, Gros P, Launay J, Temple-Boyer P (2015) PEDOT-modified integrated microelectrodes for the detection of ascorbic acid, dopamine and uric acid. Sensors Actuators B Chem 214:1–9
17. Meng A, Yuan X, Li Z, Zhao K, Sheng L, Li Q (2019) Direct growth of 3D porous $(Ni\text{-}co)_3S_4$ nanosheets arrays on rGO-PEDOT hybrid film for high performance non-enzymatic glucose sensing. Sensors Actuators B Chem 291:9–16
18. Kumar A, Gonçalves JM, Sukeri A, Araki K, Bertotti M (2018) Correlating surface growth of nanoporous gold with electrodeposition parameters to optimize amperometric sensing of nitrite. Sensors Actuators B Chem 263:237–247
19. Xin Y, Ouyang Y, Feng W, Hu Y, Yang J, Wu Z (2017) Size controllable preparation of gold nanoparticles loading on graphene sheets@cerium oxide nanocomposites modified gold electrode for nonenzymatic hydrogen peroxide detection. Sensors Actuators B Chem 238:40–47
20. Giannetto M, Mori G, Terzi F, Zanardi C, Seeber R (2011) Composite PEDOT/Au nanoparticles modified electrodes for determination of mercury at trace levels by anodic stripping voltammetry. Electroanalysis 23:456–462
21. Li Z, Yin J, Gao C, Qiu G, Meng A, Li Q (2019) The construction of electrochemical aptasensor based on coral-like poly-aniline and Au nano-particles for the sensitive detection of prostate specific antigen. Sensors Actuators B Chem 295:93–100
22. Lin P, Chai F, Zhang R, Xu G, Fan X, Luo X (2016) Electrochemical synthesis of poly(3,4-ethylenedioxythiophene) doped with gold nanoparticles, and its application to nitrite sensing. Microchim Acta 183:1235–1241
23. Fan X, Lin P, Liang S, Hui N, Zhang R, Feng J, Xu G (2017) Gold nanoclusters doped poly(3,4-ethylenedioxythiophene) for highly sensitive electrochemical sensing of nitrite. Ionics 23:997–1003
24. Zhang O, Wen Y, Xu J, Lu L, Duan X, Yu H (2013) One-step synthesis of poly(3,4-ethylenedioxythiophene)–Au composites and their application for the detection of nitrite. Synth Met 164: 47–51
25. Salsamendi M, Marcilla R, Döbbelin M, Mecerreyes D, Pozo-Gonzalo C, Pomposo JA, Pacios R (2010) Simultaneous synthesis of gold nanoparticles and conducting poly(3,4-ethylenedioxythiophene) towards optoelectronic nanocomposites. Phys Status Solidi 205:1451–1454
26. Xu J, Peng R, Ran Q, Xian Y, Tian Y, Jin L (2010) A highly soluble poly(3,4-ethylenedioxythiophene)-poly(styrene sulfonic acid)/Au nanocomposite for horseradish peroxidase immobilization and biosensing. Talanta 82:1511–1515
27. Rastgoo-Lahrood A, Martsinovich N, Lischka M, Eichhorn J, Szabelski P, Nieckarz D, Strunskus T, Das K, Schmittel M, Heckl WM (2016) From Au–thiolate chains to thioether Sierpiński triangles: the versatile surface chemistry of 1,3,5-tris(4-mercaptophenyl)benzene on Au(111). ACS Nano 10:10901
28. Lakshmi A, Anandha Raj J, Gopu G, Arumugam P, Vedhi C (2013) Electrochemical, electrochromic behaviour and effects of supporting electrolyte on nano-thin film of poly (3,4-ethylenedioxy thiophene). Electrochim Acta 92:452–459
29. Balog M, Rayah H, Le Derf F, Salle M (2008) A versatile building block for EDOT or PEDOT functionalization. New J Chem 32: 1183–1188
30. Ouyang L, Wei B, Kuo CC, Pathak S, Martin DC (2017) Enhanced PEDOT adhesion on solid substrates with electrografted P(EDOT-NH_2). Sci Adv 3:e1600448
31. Goda T, Toya M, Matsumoto A, Miyahara Y Poly(3,4-ethylenedioxythiophene) bearing phosphorylcholine groups for metal-free, antibody-free, and low-impedance biosensors specific for C-reactive protein. ACS Appl Mater Interfaces 7:27440–27448
32. Aradilla D, Estrany F, Armelin E, Alemán C (2012) Ultraporous poly(3,4-ethylenedioxythiophene) for nanometric electrochemical supercapacitor. Thin Solid Films 520:4402–4409
33. Diarisso A, Fall M, Raouafi N (2018) Elaboration of a chemical sensor based on polyaniline and sulfanilic acid diazonium salt for highly sensitive detection nitrite ions in acidified aqueous media. Environ Sci: Water Res Technol 4:1024–1034
34. Duan C, Wushuang B, Jianbin Z (2018) Non-enzymatic sensor based on a glassy carbon electrode modified with au nanoparticles/polyaniline/SnO_2 fibrous nanocomposites for nitrite sensing. New J Chem 42:11516–11524
35. Jiao M, Li Z, Li Y, Cui M, Luo X (2018) Poly(3,4-ethylenedioxythiophene) doped with engineered carbon quantum dots for enhanced amperometric detection of nitrite. Microchim Acta 185:249
36. Zhao X, Li N, Jing M, Zhang Y, Wang W, Liu L, Xu Z, Liu L, Li F, Wu N (2019) Monodispersed and spherical silver nanoparticles/graphene nanocomposites from gamma-ray assisted in-situ synthesis for nitrite electrochemical sensing. Electrochim Acta 295:434–443
37. Lu L (2019) Highly sensitive detection of nitrite at a novel electrochemical sensor based on mutually stabilized Pt nanoclusters doped CoO nanohybrid. Sensors Actuators B Chem 281:182–190
38. Nithyayini KN, Harish MNK, Nagashree KL (2019) Electrochemical detection of nitrite at NiFe2O4 nanoparticles synthesised by solvent deficient method. Electrochim Acta 317:701–710
39. Madhuvilakku R, Alagar S, Mariappan R, Piraman S (2020) Glassy carbon electrodes modified with reduced graphene oxide-MoS_2-poly (3, 4-ethylene dioxythiophene) nanocomposites for the non-enzymatic detection of nitrite in water and milk. Anal Chim Acta 1093:93–105
40. Annalakshmi M, Kumaravel S, Chen S-M, Balasubramanian P, Balamurugan TST (2020) A straightforward ultrasonic-assisted synthesis of zinc sulfide for supersensitive detection of carcinogenic nitrite ions in water samples. Sensors Actuators B Chem 305: 127387

Publisher's note Springer Nature remains neutral with regard to jurisdictional claims in published maps and institutional affiliations.